Low Temperature Physics/Fizika Nizkikh Temperatur, 2021, vol. 47, No. 12, pp. 1096–1106

Structural transformation of spin nanoclusters in low-dimensional anisotropic ferromagnets under applied magnetic field

O. V. Charkina[1], V. I. Belan[1], and M. M. Bogdan[1,2]

[1]*B. Verkin Institute for Low Temperature Physics and Engineering of the National Academy of Sciences of Ukraine Kharkiv 61103, Ukraine*
E-mail: charkina@ilt.kharkov.ua

[2]*V. N. Karazin Kharkiv National University, Kharkiv 61022, Ukraine*
E-mail: m_m_bogdan@ukr.net

Received August 13, 2021, published online October 25, 2021

Noncollinear discrete domain walls in the Heisenberg anisotropic ferromagnetic chain under applied magnetic field and their small excitation spectra are studied analytically and numerically in the framework of the Takeno–Homma equation. The intersecting frequency dependences of localized excitations and continuous spectrum oscillations and the removal of the degeneracy by the magnetic field are revealed. The variational approach is proposed to describe the domain walls and to investigate their stability. It is shown that the obtained analytical expressions fit very well the numerical solutions. The total energy of static discrete domain walls and the Peierls energy barrier between them are found explicitly. The stability diagram for noncollinear domain walls on the plane of parameters of the exchange and the magnetic field is calculated, and it looks like the alternating stripes structure of stability regions of the bond-centered and site-centered discrete domain walls. This diagram feature is explained by the oscillating dependence of the Peierls energy barrier on the exchange and the magnetic field parameters.

Keywords: anisotropic ferromagnet, exchange, magnetic field, spin nanocluster, noncollinear domain wall, stability diagram, Takeno–Homma equation.

1. Introduction

Spin nanoclusters in the quasi-one-dimensional Ising ferromagnets and resonant phenomena caused by their presence are the subject of experimental studies for a long time beginning for Ref. 1. Such a nanodomain consists of a few spins oriented oppositely to all others and separated from them by two Ising domain walls. The interaction of the cluster spins with the microwave field leads to the spin-cluster resonance, which has become a powerful research tool of magnetic properties of low-dimensional crystals [2]. It has also been shown theoretically [3–5] that the Ising domain walls can be stable in the quasi-one-dimensional Heisenberg ferromagnets with the single-ion easy-axis anisotropy of the order of the exchange. In this case the description of domain walls and their small excitations as well as stability properties has been performed in the framework of the Landau–Lifshitz equation [6]. The Ising domain wall stability makes it possible the existence of spin nanoclusters in the strongly anisotropic Heisenberg ferromagnetic chains, as predicted in [7–9].

Typical examples of quasi-one-dimensional Heisenberg ferromagnets are $CsNiF_3$ [10], possessing the excharge interaction that is significantly larger than the easy-plane anisotropy, the organometallic compounds TMNC and TMNB with the high easy-plane anisotropy that is twice more than the exchange [11, 12], and biaxial TMANC [13] and FeTAC [14] with the predominant easy-axis anisotropy. In magnetic crystals of the first type with the very weak additional easy-axis anisotropy in the easy plane the spin nanoclusters are unstable, and under applying the magnetic field they are transformed in the 360° domain walls. These spin structures can be described as solitons of the sine-Gordon (SG) equation [15], to which the Landau–Lifshitz equation is reduced in the long-wavelength limit [16]. Instead the second type and especially the third type of

ferromagnets with the biaxial anisotropy can be described by the discrete Takeno–Homma (TH) equation [17–21]. The Takeno–Homma model is formulated in terms of the azimuthal angles of spins under assumption of their small deviations from the anisotropic easy plane, and in the general case it fully takes into account the exchange interaction between neighboring spins, the in-plane anisotropy and the applied magnetic field [9, 21].

In the framework of their equation and its simpler reductions, Takeno and Homma studied numerically dynamical properties of discrete solitons and breathers, and the proximity of these nonlinear excitations to solitons of the integrable sine-Gordon equation. As a rule, in numerical simulations the exchange parameter of the Takeno–Homma reduced equations [18–20] has been chosen as the largest in comparison with the anisotropy constant and the magnetic field to make the equations close to the SG equation. In Ref. 22 the TH equation was studied numerically for one fixed value of the ratio of comparable exchange and anisotropy constants, and the noncollinear 360° domain wall and its linear oscillation modes for several values of the magnetic field parameter were found.

First, the TH equation was deduced to describe the DNA nonlinear dynamics [17, 18]. Then the model was applied to magnetic systems, crystalline polyethylene, and other plane-rotator models [19, 23]. Later, on the base of the model, Homma undertook the construction of DNA thermodynamics [24]. The majority of recent applications of the TH equation is related again to low-dimensional magnets. This is due to the appearance of new spin nano-objects, such as molecular magnetic clusters or "magnetic molecules" [25–27]. Typically, these objects are the closed ferrimagnetic and antiferromagnetic spin "wheels", which weakly interact with each other in molecular crystals. In a strong magnetic field, spins of the magnetic molecule tend to be oriented along with the magnetic field. It means that in the case of closed chains the magnetic field can change stepwise the total moment of magnetic molecules. The prospects of using these nano-objects to develop magneto-optical devices and quantum computers are associated with this property [25]. Progress in the synthesis of these magnetic molecules has led to their great diversity in size and shape: from large closed to small open chains. All this makes relevant the application of the concept of spin nanoclusters to the disordered state of the finite-size magnetic molecules and further study of their behavior in a magnetic field.

In Refs. 8, 9, authors investigated the stability and linear excitation spectra of spin nanoclusters with the Ising domain walls and found their stability boundaries as functions of a cluster size, the exchange constant and the magnetic field, as well as the explicit form of the internal oscillation modes and their local frequencies. In the present study, we concentrate on noncollinear spin structures, namely 360° discrete domain walls, in which nanoclusters are transformed after loss of stability. We have found numerically and analytically discrete soliton solutions of the TH equation, corresponding to the equilibrium domain walls with a mass center on a site and between sites, respectively, and their small excitations spectra, in particular, frequencies of internal oscillation modes. In result, we construct the stability diagram on the plane of parameters of the exchange and the magnetic field for 360° discrete domain walls and reveal its stripe structure. We find the Peierls barrier for discrete domain walls, and from it, we explain this specific feature of the stability diagram.

2. Domain walls and spin nanoclusters in the Takeno–Homma model

The Hamiltonian of the Heisenberg ferromagnetic chain with the biaxial single-ion anisotropy and the magnetic field directed along the easy-axis has the form

$$\mathcal{H} = -J\sum_n \mathbf{S}_n\mathbf{S}_{n+1} + \frac{1}{2}\sum_n \left(D(S_n^z)^2 - A(S_n^x)^2\right) - g\mu_B H\sum_n S_n^x. \tag{1}$$

Here $\mathbf{S}_n = S_0\left(\sin\theta_n\cos\varphi_n, \sin\theta_n\sin\varphi_n, \cos\theta_n\right)$ is the classical spin with the value S_0 at the nth site, φ_n and θ_n are the azimuthal and polar angles of the spin vector, respectively, J is the exchange interaction constant, A and D are the easy-axis and easy-plane anisotropy constants, respectively, H is the constant magnetic field, g is the gyromagnetic ratio, and μ_B is the Bohr magneton.

In the case of the strong easy-plane anisotropy $D >> J$, A, and small enough magnetic field with the assumption that only a weak deviation of the spin vector from the easy plane is allowed [9, 28], we reduce approximately the Hamiltonian (1) to the Hamiltonian of the Takeno–Homma model [18]:

$$\mathcal{H} = \frac{\hbar^2}{2DS_0^2}\sum_{n=1}^{N}\dot{\varphi}_n^2 - J\sum_{n=1}^{N}\cos\left(\varphi_n - \varphi_{n-1}\right) - \frac{1}{2}A\sum_{n=1}^{N}\cos^2\left(\varphi_n\right) - \frac{g\mu_0 H}{S_0}\sum_{n=1}^{N}\cos\left(\varphi_n\right). \tag{2}$$

The model is formulated in terms of only one scalar variable φ_n, and the point in the expression (2) means the differentiation with respect to time, and N is the total number of spins in the chain. The dynamics of the infinite model with the Hamiltonian (2) is described by the Takeno–Homma equation:

$$\frac{d^2\varphi_n}{dt^2} + \lambda\left(\sin\left(\varphi_n - \varphi_{n-1}\right) - \sin\left(\varphi_{n+1} - \varphi_n\right)\right) + \cos\varphi_n\sin\varphi_n + h\sin\varphi_n = 0. \tag{3}$$

The equation is presented in dimensionless form by introducing dimensionless parameters of the exchange $\lambda = J/A$

and magnetic field $h = g\mu_0 HS_0 / A$, as well as a unit of measurement of time $t_0 = \hbar/(S_0\sqrt{DA})$. In the limit, when $J >> A$, the Hamiltonian (2) is transformed into the Hamiltonian of the discrete double sine-Gordon (DDSG) model [29]. The corresponding dimensionless DDSG equation looks like

$$\frac{d^2\varphi_n}{dt^2} + \lambda\left(2\varphi_n - \varphi_{n-1} - \varphi_{n+1}\right) + \cos\varphi_n \sin\varphi_n + h\sin\varphi_n = 0. \tag{4}$$

In the long-wavelength continuum limit, when $\lambda(\varphi_{n-1} + \varphi_{n+1} - 2\varphi_n) \approx \partial^2\varphi/\partial x^2 \equiv \varphi_{xx}$ and $x = n/\sqrt{\lambda}$, from Eq. (4) the dimensionless double sine-Gordon equation follows [30]

$$\varphi_{tt} - \varphi_{xx} + \sin\varphi\cos\varphi + h\sin\varphi = 0. \tag{5}$$

In the case of the absence of magnetic field, $h = 0$, Eq. (5) is reduced to the integrable SG equation for the variable $u = 2\varphi$:

$$u_{tt} - u_{xx} + \sin u = 0. \tag{6}$$

Therefore, in terms of the azimuthal angle φ there are the π-kink and π-antikink solutions of the SG equation, which correspond to 180° domain walls of opposite signs:

$$\varphi_{\pm}(x) = 2\arctan\exp\left(\pm(x - x_0)\right), \tag{7}$$

where x_0 is a coordinate of the mass center of the domain wall.

In the nonzero magnetic field h, two identical domain walls form the static bound state, the wobbler [30], which is exact solution of Eq. (5):

$$\varphi_W(x) = 2\arctan\exp\left(\kappa_W(x - x_0) - R_W\right) + 2\arctan\exp\left(\kappa_W(x - x_0) + R_W\right). \tag{8}$$

Parameters of the wobbler are the following functions of the magnetic field parameter:

$$\kappa_W(h) = \sqrt{1+h}, \quad R_W(h) = \ln\left(\left(\sqrt{1+h} - 1\right)/\sqrt{h}\right), \tag{9}$$

where κ_W is the reverse effective length of the 180° domain wall and R_W/κ_W is a half of the wobbler width. The wobbler configuration (8) corresponds to the equilibrium 360° domain wall, which width is determined by the balance between mutual repulsion of the identical 180° domain walls and the compression effect of the magnetic field.

Noncollinear domain walls (7) and (8) arise as a consequence of the large exchange interaction. In contrast to continuous Eqs. (4)–(6), the TH equation possesses the Ising domain walls and nanocluster solutions. The spin distribution in the Ising domain wall is trivial:

$$\varphi_n^0 = 0,\ n < l;\ \varphi_n^0 = \pi,\ n \geq l, \tag{10}$$

where l denotes an arbitrary site. This solution is natural in the case of the absence of magnetic field, when the TH equation is reduced to the π-lattice sine-Gordon equation [20]:

$$\frac{d^2\varphi_n}{dt^2} + \lambda\left(\sin\left(\varphi_n - \varphi_{n-1}\right) - \sin\left(\varphi_{n+1} - \varphi_n\right)\right) + \cos\varphi_n \sin\varphi_n = 0, \tag{11}$$

when both spin directions along the easy axis correspond to the ground state of the ferromagnet. The stability problem of the domain wall (10) and the spectral problem for its linear excitations were solved in Ref. 7. Moreover, the problem of transformation of the Ising domain wall into a noncollinear structure with increasing the exchange parameter λ was solved completely for the chain consisting of four spins. In the case of large parameter λ, the internal mode frequency, which is close to the lowest edge of the continuous wave spectrum, was calculated in [31]. The problem of transformation of the complete linear excitation spectrum during the transition from collinear to noncollinear domain walls with increasing the exchange for an arbitrary chain dimension has stayed open.

In Refs. 8, 9, authors considered the collinear structure with the spin nanocluster as the following solution of the TH equation:

$$\varphi_n^0 = 0,\ n < l_1;\ \varphi_n^0 = \pi,\ -l_1 \leq n \leq l_2;\ \varphi_n^0 = 2\pi,\ n > l_2. \tag{12}$$

Spins in the nanocluster are oriented oppositely to the magnetic field direction. Evidently, the cluster width is equal to $m = l_2 - l_1 + 1$, where integers $l_2 > l_1$.

The stability and spectral problems for the spin nanocluster were solved analytically and numerically, and, finally, the stability diagram for spin clusters of an arbitrary size on the plane of parameters of the exchange and the magnetic field was found [9]. It is presented in Fig. 1.

As seen from Fig. 1, in the zero field ($h = 0$), when the ratio of the exchange constant to the easy-axis anisotropy λ reaches a critical value $\lambda_0 = 3/4$, the Ising domain boundary and in general the spin nanocluster lose stability, which

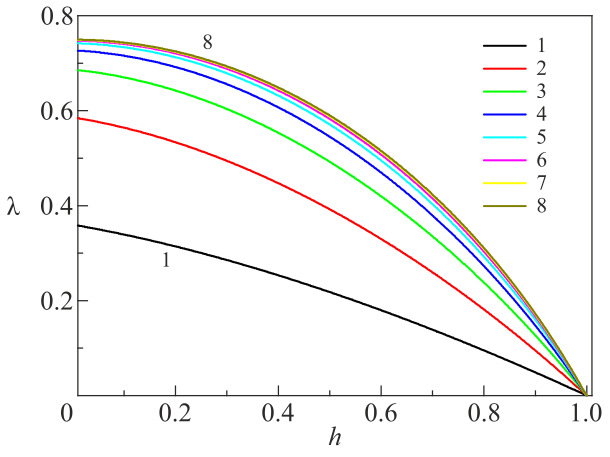

Fig. 1. (Color online) A stability diagram of nanoclusters with the number of spins between 1 and 8.

signifies the transition to the noncollinear phase. The spin nanocluster formed by two such boundaries, depending on its size and the magnetic parameters of the chain, can either transform into a 360° domain boundary, or completely fall apart into nonlinear excitations such as discrete breathers and spin waves. With increasing the parameter h the critical value of λ decreases, and for the magnetic field close to unity the spin cluster abruptly decays.

In general, in order to solve the stability problem for any static solution φ_n^0 of the TH equation, it is necessary to find a spectrum of its small excitations, i.e., to solve the linearized equation for the small addition $\Delta\varphi_n(t)$ to the solution:

$$\Delta\varphi_n(t) = \varphi_n(t) - \varphi_n^0 << 1, \quad \Delta\varphi_n(t) = \psi_n \exp(i\omega t), \qquad (13)$$

which is reduced to the eigenvalue problem with the squared frequency spectral parameter ω^2:

$$\lambda\left((\psi_n - \psi_{n-1})\cos(\varphi_n^0 - \varphi_{n-1}^0) - (\psi_{n+1} - \psi_n)\cos(\varphi_{n+1}^0 - \varphi_n^0)\right) + \left(\cos 2\varphi_n^0 + h\cos\varphi_n^0\right)\psi_n = \omega^2\psi_n . \qquad (14)$$

In the next sections, we presented numerical and analytical results of the calculation of noncollinear spin structures, which described by the TH equation, and their oscillatory and stability properties.

3. Small oscillations of noncollinear domain walls in weak magnetic fields

We start from the above-mentioned spectral problem for the 180° domain wall in the case of the absence of a magnetic field, which is described by the π-lattice sine-Gordon equation (10). The critical value of the exchange parameter λ_0 of the transition from collinear to noncollinear domain wall in the infinite chain coincides for both the Landau–Lifshitz and TH equations. For the 4-spins chain, such a value is smaller: $\lambda_* = 1/\sqrt{2} \approx 0.707$ [7], but for the number of spins N more than 7, it already reaches practically the limit value λ_0. Therefore, we consider the finite-size chain of 8 spins with open edges and, after direct substitution of the spin distribution (10) into Eq. (14), easily find numerically eigenvalues of the spectral problem for parameter λ less than λ_0. The first six squared frequencies are shown in Fig. 2. The behavior of the internal modes of the Ising domain wall was analyzed in [7, 8]. The homogeneous in-phase oscillation determines the lowest frequency edge ω_0 of continuum spectrum, which number of modes increases with increasing the number of spins. The antiphase mode dependence begins from the edge frequency ω_0 and tends to zero at λ_0.

In order to obtain a noncollinear domain wall as a static solution of Eq. (11), we use the usual relaxation method consisting in solving the modified equation after the formal change of the second-order temporal derivative in Eq. (11) by the first-order derivative, which means introducing

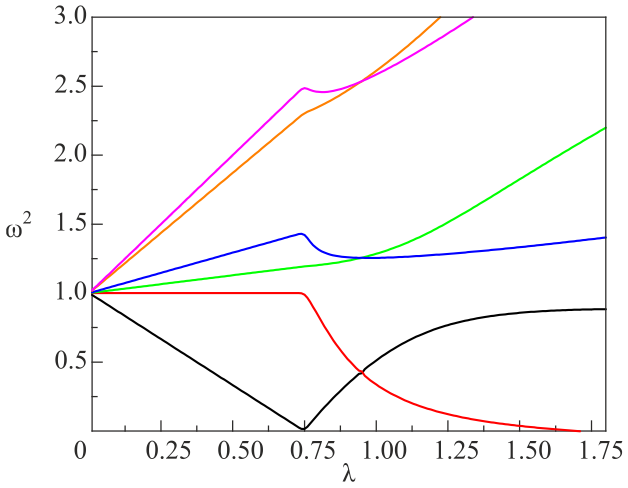

Fig. 2. (Color online) The intersecting frequency dependences of internal and continuum spectrum modes of the 180° noncollinear domain wall.

the effective dissipation. We use the Ising domain wall spin configuration as the initial condition, and after dozen of iterations, we obtain the equilibrium noncollinear spin distribution with very high accuracy. This method has been employed throughout our research. After substitution of the noncollinear solution into Eq. (14), we calculate the dependences of the squared frequencies on the parameter λ for values more than λ_0. They are also shown in Fig. 2. After transformation of the domain wall into the noncollinear structure, we reveal that in the finite-size open chain, the frequencies of pairs of internal modes and continuum spectrum oscillations have the unified intersection point. In other words, the "crossing situation" takes place [32]. This point is equal to $\lambda_{cr} \approx 0.95$ and practically does not change with increasing the chain dimension more than 8 spins, while for the 4-spins system it equals 0.838.

The oscillatory properties of the spin nanoclusters at a small magnetic field we discussed in detail in Ref. 9. Now we concentrate on changing the small excitations spectrum after transformation of the cluster into the 360° domain wall. In order to find the noncollinear structure for the static TH equation (3), in the relaxation scheme we choose the initial condition in the form (12) with the cluster size $m = 8$ and the total number of spins in the open chain $N = 24$. As an example, the resulting spin configuration is shown in Fig. 3 for the case when the exchange and magnetic field parameters are chosen as $\lambda = 1$ and $h = 0.01$, respectively. As seen in Fig. 3, the spin structure is similar to the wobbler configuration (8) with the well-separated 180° discrete domain walls. Its center of mass is located between sites, so that the domain wall is bond-centered.

For this fixed value of the magnetic parameter we calculated noncollinear spin configurations for a wide range of the parameter λ and then solved the eigenvalue problem (14). The squared frequency dependences of the internal modes

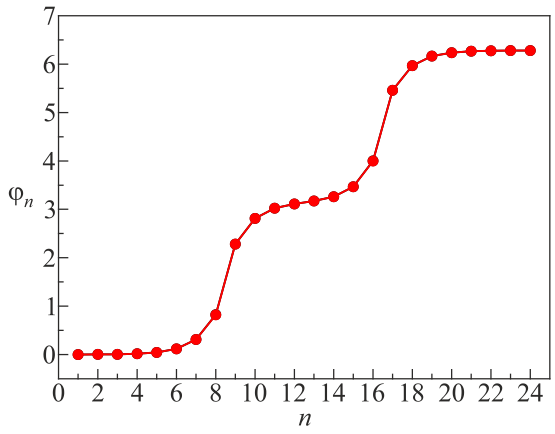

Fig. 3. The discrete 360° domain wall with a center of mass between sites at $\lambda = 1$ and $h = 0.01$.

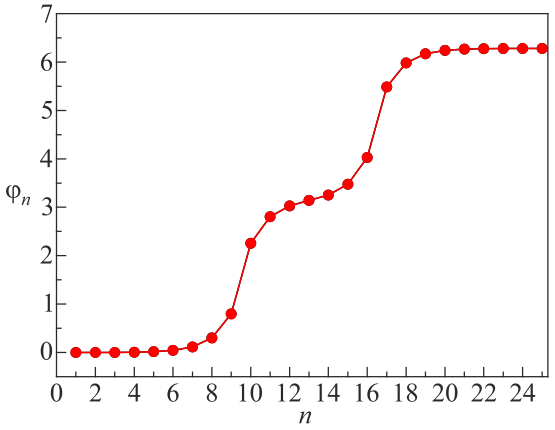

Fig. 5. The discrete 360° domain wall with center of mass on site at $\lambda = 1$ and $h = 0.025$.

and continuum oscillation spectrum of the spin cluster and the 360° domain wall on the exchange parameter are shown in Fig. 4. As seen in Fig. 4, the presence of two 180° domain walls, composing the nanocluster, leads to splitting the dependences of the internal mode frequencies. However, the main effect is the removal of the crossing situation [32], i.e., the removal of the frequency degeneracy at the point λ_{cr} by the hybridization of internal oscillations and the formation of the frequency gap. In the vicinity of the critical point the character of every mode changes drastically. In result, with increasing the exchange parameter after the critical point λ_{cr} four frequency dependences of the internal modes behave as the following: the lowest tends to zero and leads to the domain wall instability, the second and the third exist in the gap, and highest tends to the continuum spectrum. This result is in agreement with numerical calculations of the internal mode frequencies of the wobbler-like structure in the DDSG equation [29] and explains the origin of localized oscillation modes of the DDSG wobbler.

For the comparison, we also present analogous figures for the chain with the odd number of spins, namely $N = 25$, and for the larger field parameter $h = 0.025$. The localized excitation spectrum of the nanocluster in this chain has been discussed in detail in Ref. 9. The spin distribution of the 360° domain wall with a mass center on the node is shown in Fig. 5.

The internal modes and continuum oscillation spectrum are presented in Fig. 6. Comparing Figs. 4 and 6, we see that the more the magnetic field, the more the gap between internal mode frequencies after the removal of their degeneracy.

The above results suggest that the wobbler expression (8) would be a good variational approximation of the discrete 360° domain wall after returning from the continuous coordinate x to discrete node's numbers. Such a variational ansatz can be chosen in the form

$$\varphi_V(n) = 2\arctan\exp\left(\kappa(n-n_0)-R\right) + 2\arctan\exp\left(\kappa(n-n_0)+R\right), \qquad (15)$$

where κ and R are variational parameters, and $n_0 = 0$ or $n_0 = 1/2$ if a center of mass the 360° domain wall is located on site or between sites, respectively. The equivalent form of the ansatz (15) looks like

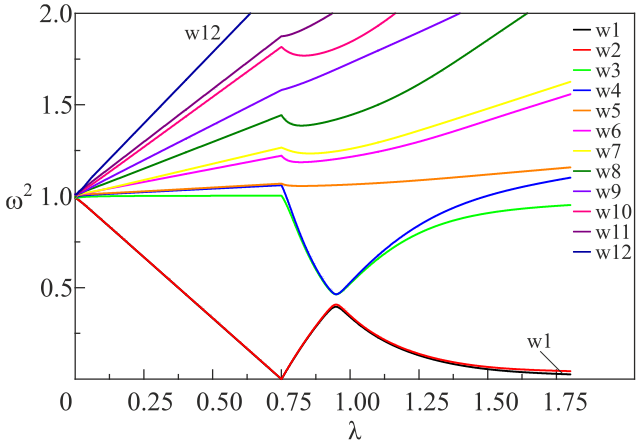

Fig. 4. (Color online) The internal modes and continuum oscillation spectrum of the spin cluster and the bond-centered 360° domain wall at $h = 0.01$.

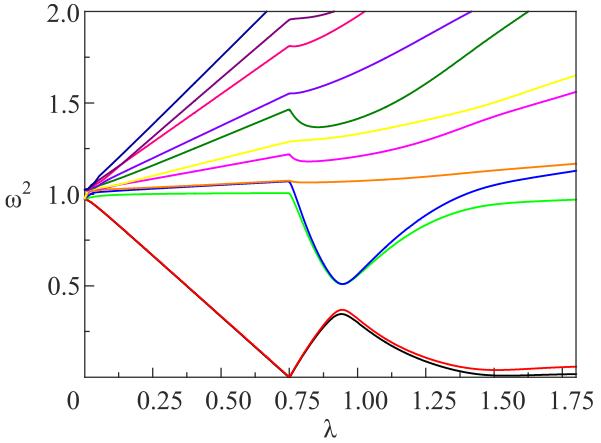

Fig. 6. (Color online) The internal modes and continuum oscillation spectrum of the spin cluster and the center-on-site 360° domain wall at $h = 0.025$.

$$\varphi_V(n) = \pi + 2\arctan\left(\frac{\sinh\kappa(n-n_0)}{\cosh R}\right). \qquad (16)$$

The expression (15) or (16) would be an approximate solution of the TH equation if the parameter values κ and R correspond to the minimum of the potential energy written in the dimensionless form:

$$E = \lambda\sum_{n=-\infty}^{\infty}\left(1-\cos\left(\varphi_n-\varphi_{n-1}\right)\right)$$
$$+\frac{1}{2}\sum_{n=-\infty}^{\infty}\left(1-\cos 2\varphi_n\right)+h\sum_{n=-\infty}^{\infty}\left(1-\cos\varphi_n\right). \qquad (17)$$

Thus, the proposed variation procedure consists in the substitution of the ansatz into Eq. (17) and finding the explicit expression $E(\kappa, R)$ and seeking for local minima of this function for the static spin configurations with $n_0 = 0$ or $n_0 = 1/2$. Before application of the variation procedure, in the next section we study analytically and numerically the case of high magnetic fields.

4. Noncollinear domain walls at high magnetic fields

The TH equation in the case of magnetic fields much exceeding the anisotropy, i.e., $h >> 1$, is reduced to the following equation:

$$\frac{d^2\varphi_n}{dt^2}+\lambda\left(\sin\left(\varphi_n-\varphi_{n-1}\right)-\sin\left(\varphi_{n+1}-\varphi_n\right)\right)+h\sin\varphi_n = 0. \qquad (18)$$

As easily seen, the static solutions of this equation depend only on a single parameter $a^2 \equiv h/\lambda$. Assuming that the exchange is much more than a magnetic field, $a << 1$, we go to the long-wavelength limit and can substitute in Eq. (18) instead the exchange terms the following expression:

$$\sin\left(\varphi_n-\varphi_{n-1}\right)+\sin\left(\varphi_n-\varphi_{n+1}\right)$$
$$\Rightarrow -a^2\varphi_{xx}-\frac{a^4}{12}\varphi_{xxxx}+\frac{a^4}{2}\varphi_x^2\,\varphi_{xx}, \qquad (19)$$

where $x = an$ is the continuous coordinate. In result, we deduce the ordinary nonlinear differential equation

$$\varphi_{xx}-\sin\varphi = a^2\left(\varphi_x^2\varphi_{xx}-\frac{1}{6}\varphi_{xxxx}\right). \qquad (20)$$

The approximate solution of Eq. (20) is obtained, using the smallness of the parameter a^2 and the perturbation theory of Ref. 33, in the form of the compressed 4π-kink:

$$\varphi(x) = 4\arctan\exp(x)-\frac{a^2}{4}\left(\frac{1}{3}\frac{x}{\cosh x}-5\frac{\sinh x}{\cosh^2 x}\right). \qquad (21)$$

In Ref. 33, it has been shown that the solution like Eq. (21) can be considered as the small parameter expansion of the expression

$$\varphi = 2\arctan\exp\left(\kappa_0 x-i\delta_0\right)+2\arctan\exp\left(\kappa_0 x+i\delta_0\right) \qquad (22)$$

with the specific values of its parameters: $\kappa_0 = 1-a^2/24$ and $\delta_0 = \sqrt{5}a/2$. Although $\kappa_0 < 1$ means that the π-kink width increases but the larger parameter δ_0 leads to steepening the 360° domain wall [33]. The expression (22) prompts the following variational ansatz for the discrete 360° domain wall in high magnetic fields:

$$\varphi_V(n) = 2\arctan\exp\left(\kappa(n-n_0)-i\delta\right)$$
$$+2\arctan\exp\left(\kappa(n-n_0)+i\delta\right), \qquad (23)$$

or its equivalent form:

$$\varphi_V(n) = \pi + 2\arctan\left(\frac{\sinh\kappa(n-n_0)}{\cos\delta}\right). \qquad (24)$$

Comparing Eq. (24) with Eq. (16), we can joint these two expression in the unified ansatz:

$$\varphi_V(n) = \pi + 2\arctan\left(\frac{\sinh\kappa(n-n_0)}{A}\right) \qquad (25)$$

with the variational parameter A, which changes from small values to unity $A = \cos\delta \le 1$, describing the compressed discrete 360° domain wall, and from unity to large values $A = \cosh R \ge 1$, describing the wobbler-like structure of two discrete 180° domain walls. In the next section we apply the variational procedure to find approximate noncollinear discrete domain wall solutions and to study analytically their stability properties.

5. The Peierls barrier and stability diagram of domain walls in the TH equation

First, we show that the variational approach leads to satisfactory approximate solutions of the TH equation for the discrete 360° domain walls. Introducing a discrete variable $z_n = \kappa(n-n_0)$ after substitution of the ansatz (25) into the energy expression (17), we obtain the expression

$$E = 2A\left(\lambda\sum_n\frac{\left(\sinh z_n-\sinh z_{n-1}\right)^2}{\left(\sinh^2 z_n+A\right)\left(\sinh^2 z_{n-1}+A\right)}\right.$$
$$\left.+\sum_n\frac{\sinh^2 z_n}{\left(\sinh^2 z_n+A\right)^2}+h\sum_n\frac{1}{\sinh^2 z_n+A}\right). \qquad (26)$$

It is appeared that the energy dependence can be calculated analytically by the use of the Poisson's formula [32]:

$$\sum_{n=-\infty}^{\infty}f(n) = \sum_{m=-\infty}^{\infty}\int_{-\infty}^{\infty}f(k)\exp(2\pi imk)\,dk. \qquad (27)$$

All the integrals are found exactly, and the energy can be presented as the sum of four contributions:

$$E = E_0 + E_P^{\text{ex}} + E_P^{\text{an}} + E_P^{Z}. \qquad (28)$$

The term E_0 is the part that is independent of n_0. The results of the integration are different for the parameters $A = \cosh R \geq 1$ and $A = \cos\delta \leq 1$. We obtain the following expression for the wobbler-like configuration:

$$E_0(\kappa, R) = \frac{2}{\kappa}\left(4\lambda \frac{\dfrac{2R}{\sinh 2R} + \dfrac{\kappa}{\sinh\kappa}}{\coth^2\dfrac{\kappa}{2} - \tanh^2 R} + 2hR\coth R \right.$$

$$\left. + \coth R\left(\coth R - \frac{R}{\sinh^2 R}\right)\right), \qquad (29)$$

and for the compressed 360° domain wall, respectively:

$$E_0(\kappa, \delta) = \frac{2}{\kappa}\left(4\lambda \frac{\dfrac{2\delta}{\sin 2\delta} + \dfrac{\kappa}{\sinh\kappa}}{\coth^2\dfrac{\kappa}{2} + \tan^2\delta} + 2h\delta\cot\delta \right.$$

$$\left. + \cot\delta\left(\frac{\delta}{\sin^2\delta} - \cot\delta\right)\right). \qquad (30)$$

Now we are able to demonstrate the next step of the variational approach. Possessing the explicit expression $E_0(\kappa, R)$, it is easy to reveal a local minimum of this function and to determine corresponding minimum "coordinates" $\kappa_{\min}$ and $A_{\min}$. In Fig. 7, we show the surface $E(\kappa, R)$ and sections near its local minimum. The sought-for point is contained inside the elliptic contour.

There are a lot of algorithms to find the minimum point. We use a simple iteration scheme: starting from the initial R_0, we calculate $E(\kappa, R_0)$, and after finding the derivative analytically, we solve the equation $\partial E(\kappa, R_0)/\partial\kappa = 0$ to obtain κ_1. Further we calculate $E(\kappa_1, R)$, and after finding the derivative, we solve the equation $\partial E(\kappa_1, R)/\partial R = 0$ to obtain R_1, etc. Thus, due to the rapidly converging scheme, we find the sought-for values of the minimum "coordinates" $\kappa_{\min}$ and $R_{\min}$ for the fixed values of the parameters λ and h. As examples, we present in Fig. 8 the exact numerical domain wall solutions, which have been found by the relaxation method, starting from the wobbler initial condition, and the variational expressions with the calculated parameters. As seen, the numerical and variational solutions are indistinguishable by eye in contrast to the initial condition profile.

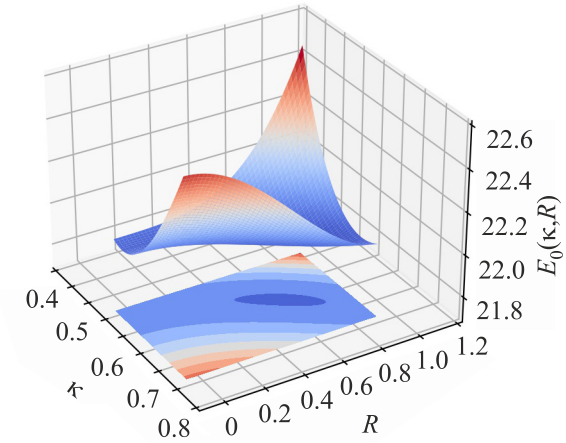

Fig. 7. (Color online) The energy dependence $E_0(\kappa, R)$ for the case $\lambda = 6$ and $h = 1$.

Returning to Eqs. (27) and (28), we recall that from a whole set of harmonics with $m \neq 0$ in the Poisson's formula the first is much larger than others [32], therefore we write out only this one in contributions given by the exchange interaction, the anisotropy and the Zeeman energy: E_P^{ex}, E_P^{an} and E_P^Z, respectively. Below these contributions are presented for the case $A > 1$:

$$E_P^{\text{ex}} = \frac{16\pi}{\kappa}\frac{\lambda}{\left(\coth^2\dfrac{\kappa}{2} - \tanh^2 R\right)}\frac{1}{\sinh 2R}\frac{\sin\left(\dfrac{2\pi}{\kappa}R\right)}{\sinh\dfrac{\pi^2}{\kappa}}\cos(2\pi n_0), \qquad (31)$$

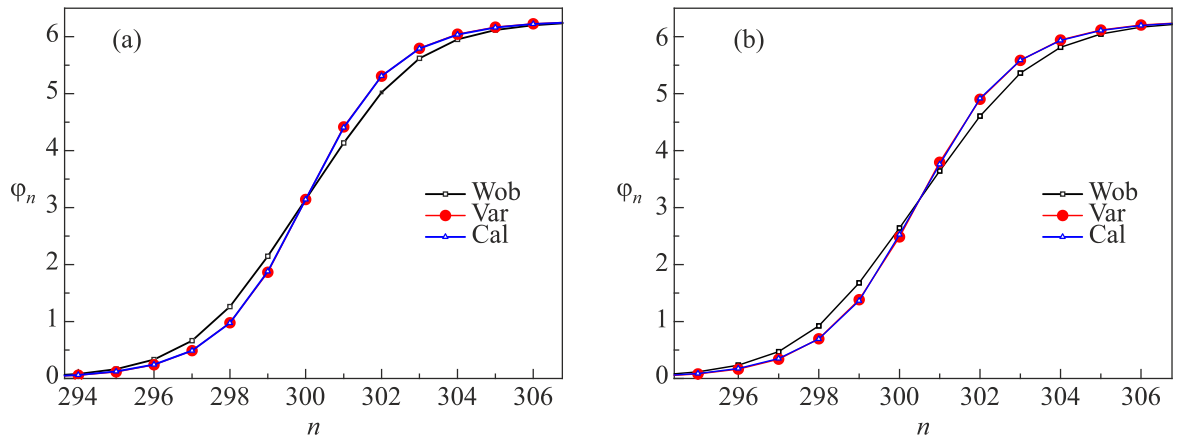

Fig. 8. (Color online) The profiles of the initial wobbler configuration (Wob), variational (Var) and numerical (Cal) solutions for 360° discrete domain walls with a center of mass on site (a) and between sites (b) for the parameters $\lambda = 4$ and $h = 1$.

$$E_P^{\text{an}} = \frac{2\pi}{\kappa}\coth R\left(\frac{2\pi}{\kappa}\coth R\cos\left(\frac{2\pi}{\kappa}R\right)-\frac{\sin\left(\frac{2\pi}{\kappa}R\right)}{\sinh^2 R}\right)$$
$$\times\frac{\cos(2\pi n_0)}{\sinh\frac{\pi^2}{\kappa}}, \qquad (32)$$

$$E_P^Z = \frac{4\pi}{\kappa}h\coth R\frac{\sin\left(\frac{2\pi}{\kappa}R\right)}{\sinh\frac{\pi^2}{\kappa}}\cos(2\pi n_0). \qquad (33)$$

The small additions (31)–(33) to the energy E do not practically influence on the functional form of the solutions, but they define the stability properties of noncollinear discrete domain walls. As seen from the formulas, two equilibrium spin configurations with $n_0 = 0$ or $n_0 = -1/2$ are separated by the Peierls energy barrier:

$$E_B = \frac{4\pi}{\kappa\sinh\frac{\pi^2}{\kappa}}\left(\left(2h\coth R+\frac{8\lambda}{\sinh 2R}\frac{1}{\left(\coth^2\frac{\kappa}{2}-\tanh^2 R\right)}\right)\right.$$
$$\left.\times\sin\left(\frac{2\pi}{\kappa}R\right)+\coth R\left(\frac{2\pi}{\kappa}\coth R\cos\left(\frac{2\pi}{\kappa}R\right)-\frac{\sin\left(\frac{2\pi}{\kappa}R\right)}{\sinh^2 R}\right)\right). \qquad (34)$$

For the wobbler-like solutions of the TH equation, the function $E_B(\kappa, R)$ is shown in Fig. 9. We see that for not small values of the parameter $\kappa \le 1$ and $R > 1$ the function oscillates and changes sign.

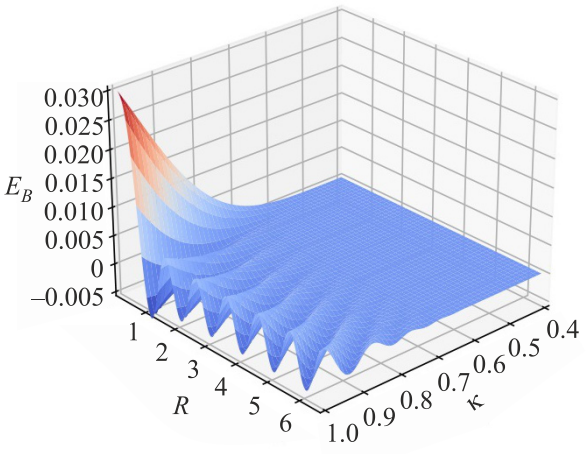

Fig. 9. (Color online) The dependence of the energy barrier E_B between of two equilibrium wobbler-like configurations with $n_0 = 0$ or $n_0 = -1/2$ on the parameters κ and R.

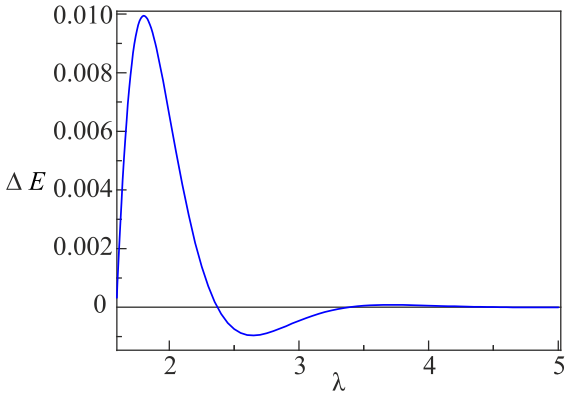

Fig. 10. (Color online) The oscillating energy barrier between discrete domain walls as the function of the parameter λ for the parameter $h = 0.15$.

In order to make sure that the Peierls barrier, separating domain walls, can change sign, we have calculated the parameters $\kappa_{\min}$ and $R_{\min}$ as a function of the exchange parameter λ for the fixed value of the parameter $h = 0.15$. Then we have found the energy difference ΔE between the obtained variational solutions as a function of λ. This oscillating dependence is shown in Fig. 10. As seen in figure, the function $\Delta E(\lambda)$ equals zero in a sequence of points: 1.59, 2.36, 3.4, 4.6, etc. These points define the boundaries of stability and instability of domain walls with different positions of a center of mass. In the region of parameter λ between 1.59 and 2.36, the domain wall with a center of mass between sites is stable, and the domain wall with a center of mass on site is unstable, and in the next interval vice versa, etc.

These analytical results are confirmed by direct numerical calculations of solutions of the TH equation within the relaxation method, starting from the wobbler-like ansatz, and finding the spectrum of linear excitations of the domain walls to establish the instability modes and the parameter values of their "smoothing", i.e., the frequency vanishing. Thus, we have constructed the stability diagram of the noncollinear discrete domain walls on the plane of parameters λ and h, which is shown in Fig. 11. The dia-

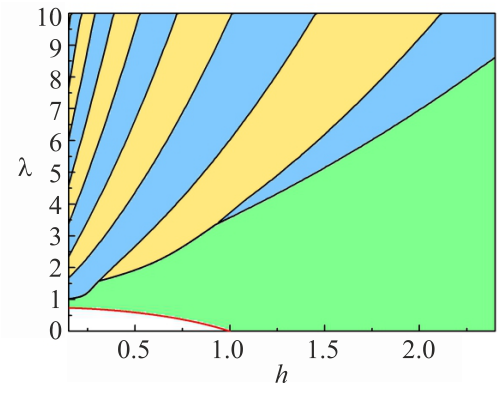

Fig. 11. (Color online) The stability diagram of the noncollinear discrete domain walls on the plane of the parameters λ and h.

gram has a stripe structure where the yellow regions denote the stability zones of the center-on-bond domain walls and the blue regions to the stability zones of the center-on-site domain walls, respectively. The left edge of the diagram is chosen to be equal to $h = 0.15$, and we see that boundary points on the ordinate axis coincide well with the sequence of zeros of the function $\Delta E(\lambda)$ from Fig. 10. It is interesting to note that the solutions presented in Fig. 9 lie on the stability boundary on the diagram and their energies are equal. The region of the stability of spin nanoclusters, presented in detail in Fig. 1, is denoted in the diagram by white colour. The green colour denotes the region where no static domain structures exist. In the relaxation scheme they disappear, i.e., ferromagnet falls down in the ground state, but in the nondissipative TH equation they decay into discrete breathers and spin waves. The general form of the limit boundaries of the instability of spin clusters and noncollinear domain walls, including small and large magnetic fields, has already been presented in Fig. 7 of Ref. 9 on a logarithmic scale. The region of the exchange parameter λ of the order of unity above the nanocluster instability boundary at small fields contains a variety of inhomogeneous solutions including domain walls with different numbers of spins in their central parts, soliton-antisoliton structures, etc. They are obtained from different initial conditions and turn out to be stable, leading to the wedge-shaped stability boundaries like that in Fig. 11 for 360° domain walls. Therefore, obtainment of the complete pattern of the stability of all inhomogeneous solutions needs more detailed research.

On the other hand, if the initial spin distributions would be well and lead to the ansatz-like structures for large λ and h, but they can work worse for small values of the parameters and differ significantly from the final states. In this case, the calculated energy and the domain wall contribution to the magnetization $M = \sum_{n=-\infty}^{\infty} (1 - \cos\varphi_n)$ look like dependences shown in Fig. 12. While for the relatively large λ the energy dependences are smooth and monotonic and the magnetization curves have only small steps, then for the smaller exchange all the dependences become stepwise and reflect the jumping transition between metastable spin configurations.

At last, note that we do not regard in general extremely small values of the exchange parameter λ, when one has to keep in mind the problem of the anticontinuum limit [34], i.e., the limit of weakly coupled spins, when the parameter λ vanishes. In the anti-integrable limit, there are chaotic trajectories in the mappings to which the TH equations are reduced in the static case [18]. The relaxation method allows to get these metastable spin states, corresponding to the local energy minima, but the final results crucially depend on the initial spin configurations. They correspond to the spin distributions with the random spatial sequence of the spin directions along and opposite to the easy axis and cannot be obtained within the analytical approach.

Conclusion

The static topological spin structures in the quasi-one-dimensional anisotropic Heisenberg ferromagnets have been studied analytically and numerically in the framework of the Taken–Homma equation under applying the magnetic fields. This model describes well the known easy-plane and biaxial ferromagnets such as $CsNiF_3$ TMNC, FeTAC and their modifications. The importance of the stable static spin configurations is defined by their contributions to the configurational partition function, and hence to thermodynamic properties, which manifest themselves in the low-temperature experiments with the quasi-one-dimensional magnets and crystals with magnetic molecular nanoclusters, so-called magnetic molecules. We have investigated the structural conversion of the spin nanodomain bounded by the Ising domain walls into the noncollinear discrete 360° domain wall and traced the transformation of spectra of localized and propagated excitations of these spin configurations under the action of a magnetic field applied along the easy axis.

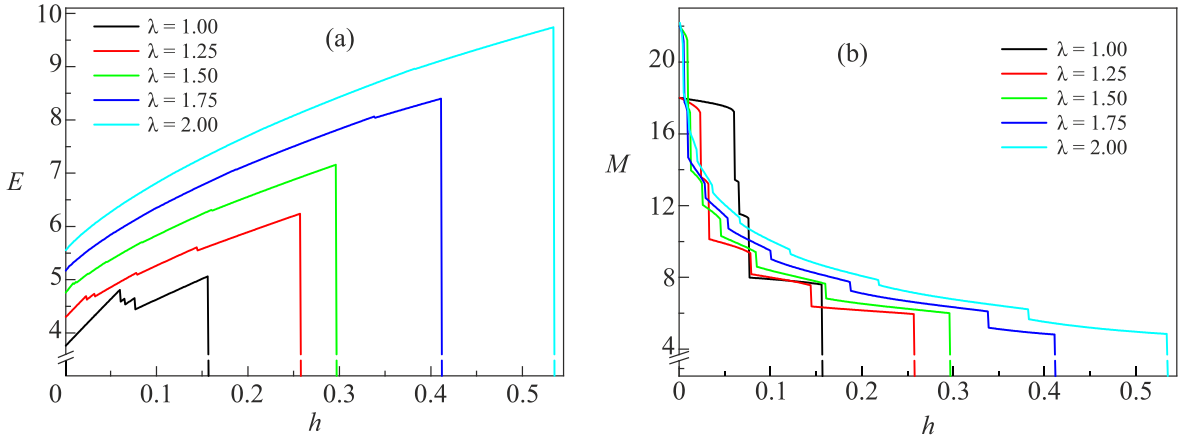

Fig. 12. (Color online) The dependences of the energy (a) and the domain wall contribution to the magnetization (b) on the magnetic field for different values of the exchange parameter.

We have found the intersecting frequency dependences of internal modes and continuum spectrum excitations of noncollinear 180° and 360° domain walls and established the removal of the degeneracy by the magnetic field. We have proposed the variational ansatz for the discrete 360° domain wall solutions of the Takeno–Homma equation and used the variation procedure to obtain approximate solutions which are indistinguishable from exact numerical solutions for a wide range of the exchange and magnetic field parameters. It has allowed to calculate the analytical expression for the total energy of the domain structure and found the Peierls energy barrier between discrete 360° domain walls with the spin configuration center on site and between sites. This energy difference turns out to be the oscillating and changing sign function of the exchange and the magnetic field. This property of the Peierls barrier prompts the alternation of the stability regions of two kinds of the equilibrium domain walls. We have calculated by the relaxation method the exact solutions for the domain walls and found their instability modes and points of their frequency vanishing. In result, we have built the stability diagram for noncollinear domain walls on the plane of parameters of the exchange and the magnetic field and revealed the predicted alternating stripes structure of the stability regions of two types of the equilibrium discrete 360° domain walls with the configuration center on site and between sites. The obtained results concerning the behavior of the internal mode frequencies of the 180° and 360° discrete domain walls of the Takeno–Homma equation explain the origin and specific features of spectra of internal modes of discrete solitons in the sine-Gordon equation and the double sine-Gordon equation, which are regarded as the limit cases of the Takeno–Homma equation.

Acknowledgments

This work was performed using computational facilities of grid-cluster ILTPE — B. Verkin Institute for Low Temperature Physics and Engineering of the National Academy of Sciences of Ukraine.

1. M. Date and M. Motokawa, *Phys. Rev. Lett.* **16**, 1111 (1966).
2. M. Date and M. Motokawa, *J. Phys. Soc. Jpn.* **24**, 41 (1968).
3. J. J. van den Broek and H. Zijlstra, *IEEE Trans. Magn. MAG* **7**, 226 (1971).
4. A. N. Goncharuk, A. A. Stepanov, and D. A. Yablonsky, *Fiz. Tverd. Tela* **31**, 132 (1989) [*Sov. Phys. Solid State* **31**, 2099 (1989)].
5. M. V. Gvozdikova, A. S. Kovalev, and Yu. S. Kivshar, *Fiz. Nizk. Temp.* **24**, 635 (1998) [*Low Temp. Phys.* **24**, 479 (1998)].
6. A. M. Kosevich, B. A. Ivanov, and A. S. Kovalev, *Phys. Rep.* **194**, 117 (1990).
7. M. V. Gvozdikova and A. S. Kovalev, *Fiz. Nizk. Temp.* **25**, 1295 (1999) [*Low Temp. Phys.* **25**, 972 (1999)].
8. O. V. Charkina and M. M. Bogdan, *Fiz. Nizk. Temp.* **44**, 824 (2018) [*Low Temp. Phys.* **44**, 644 (2018)].
9. M. M. Bogdan, V. I. Belan, and O. V. Charkina, *Fiz. Nizk. Temp.* **44**, 1700 (2018) [*Low Temp. Phys.* **44**, 1331 (2018)].
10. A. P. Ramirez and W. P. Wolf, *Phys. Rev. Lett.* **49**, 227 (1982).
11. C. Dupas and J. P. Renard, *J. Phys. C* **10**, 5057 (1977).
12. L. J. de Jongh, C. A. M. Mulder, H. M. Cornelisse, A. J. van Duyneveldt, and J. P. Renard, *Phys. Rev. Lett.* **47**, 1672 (1981).
13. A. G. Anders, S. V. Volotsky, V. G. Borisenko, and Yu. V. Pereverzev, *Fiz. Nizk. Temp.* **15**, 39 (1989) [*Sov. J. Low Temp. Phys.* **15**, 21 (1989)].
14. R. S. Rubins, T. D. Black, A. Sohn, and J. E. Drumheller, *Phys. Rev. B* **49**, 15366 (1994).
15. H.-J. Mikeska and M. Steiner, *Adv. Phys.* **40**, 191 (1991).
16. H. J. Mikeska, *J. Phys. C* **11**, L29 (1978).
17. S. Takeno and S. Homma, *Prog. Theor. Phys.* **70**, 308 (1983).
18. S. Homma and S. Takeno, *Prog. Theor. Phys.* **72**, 679 (1984).
19. S. Takeno and S. Homma, *J. Phys. Soc. Jpn.* **55**, 65 (1986).
20. S. Takeno and S. Homma, *J. Phys. Soc. Jpn.* **55**, 2547 (1986).
21. S. Homma and S. Takeno, *Prog. Theor. Phys.* **74**, 618 (1985).
22. V. V. Beloshapkin, G. P. Berman, A. G. Tretyakov, and E. V. Shtukkert, *JETP* **100**, 1238 (1991) [*Sov. Phys. JETP* **73**, 683 (1991)].
23. C. Etrich, H. J. Mikeska, E. Magyari, H. Thomas, and R. Weber, *Phys. B* **62**, 97 (1985).
24. S. Homma, *Physica D* **113**, 202 (1998).
25. D. Gatteschi, R. Sessoli, and J. Villain, *Molecular Nanomagnets*, Oxford University Press, New York (2006).
26. V. V. Kostyuchenko, I. M. Markevtsev, A. V. Philippov, V. V. Platonov, V. D. Selemir, O. M. Tatsenko, A. K. Zvezdin, and A. Caneschi, *Phys. Rev. B* **67**, 184412 (2003).
27. A. Müller, M. Luban, C. Schröder, R. Modler, P. Kögerler, M. Axenovich, J. Schnack, P. Canfield, S. Bud'ko, and N. Harrison, *Chem. Phys. Chem.* **2**, 517 (2001).
28. M. M. Bogdan and O. V. Charkina, *Fiz. Nizk. Temp.* **47**, 483 (2021) [*Low Temp. Phys.* **47**, 449 (2021)].
29. P. Tchofo Dinda and C. R. Willis, *Phys. Rev. B* **51** 4958 (1995).
30. D. K. Campbell, M. Peyrard, and P. Sodano, *Physica D* **19**, 165 (1986).
31. Fei Zhang, *Physica D* **110**, 51 (1997).
32. A. M. Kossevich, *The Crystal Lattice* (*Phonons, Solitons, Dislocations*), WILEY-VCH Verlag Berlin GmBH, Berlin (1999).
33. M. M. Bogdan and O. V. Charkina, *Fiz. Niz. Temp.* **47**, 173 (2021) [*Low Temp. Phys.* **47**, 155 (2021)].
34. S. Aubry and G. Abramovici, *Physica D* **43**, 199 (1990).

Структурна трансформація спінових нанокластерів у низьковимірних анізотропних феромагнетиках під дією магнітного поля

O. V. Charkina, V. I. Belan, M. M. Bogdan

Аналітично та чисельно досліджуються неколінеарні дискретні доменні стінки та спектри їх малих збуджень у гейзенбергівському анізотропному феромагнітному ланцюжку під дією магнітного поля в рамках рівняння Такено–Хомма. Виявлено частотні залежності локалізованих збуджень та коливань безперервного спектра, що перетинаються, та усунення такого виродження магнітним полем. Запропоновано варіаційний підхід для опису доменних стінок та дослідження їх стійкості. Показано, що отримані аналітичні вирази дуже добре узгоджуються з чисельними розв'язками. Знайдено явно повну енергію статичних дискретних доменних стінок та енергетичний бар'єр Пайерлса між ними. Розраховано діаграму стійкості для неколінеарних доменних стінок на площині параметрів обміну та магнітного поля, яка виглядає як смугаста структура областей стабільності дискретних доменних стінок із центром на вузлі та центром між вузлами. Ця особливість діаграми пояснюється осцилюючою залежністю енергетичного бар'єра Пайерлса від параметрів обміну та магнітного поля.

Ключові слова: анізотропний феромагнетик, обмін, магнітне поле, спіновий нанокластер, неколінеарна доменна стінка, діаграма стійкості, рівняння Такено–Хомма.